

# Investigation of Dislocations Introduced in Si Wafer during Flash Lamp Annealing by Photoluminescence Spectroscopy

Diana Ryzhak,<sup>\*</sup> Gudrun Kissinger, Andreas Ehlert, Andreas Sattler, Davide Spirito, and Dawid Kot

Dislocations are generated in Si wafers during flash lamp annealing for 20 ms. The samples have been etched to different depths and macro-photoluminescence (PL) spectra have been recorded for different dislocation densities. A micro-PL investigation is also carried out on a cross section of a sample. Four characteristic emission peaks are found, which are the well-known D1, D2, D3, and D4 lines. The findings demonstrate a significant influence of the defect densities on the PL spectra of the D lines by using both the micro- and the macro-PL setups, and show a correlation of the PL intensities with etch pit density measured against the depth of the wafer. Additionally, the D lines dependency on temperature is explored, offering insights into the underlying mechanisms. The D lines exhibit a pronounced temperature dependence, which can be attributed to various factors including phonon interactions and thermal expansion effects. The influence of nickel contamination is also examined.

labeled as D1, D2, D3, and D4 lines in the energy range 0.8–1 eV. The main theory regarding the origin of the D lines in Si, as explored by Kittler,<sup>[4]</sup> Tajima,<sup>[5]</sup> and their contemporaries, centers on the role of dislocations and their interaction with impurities within the Si lattice, particularly transition metals. The research by Sugimoto et al.<sup>[6]</sup> shows that D lines, specifically D1–D4, are observable only in areas with defects, suggesting that these dislocations themselves are active as radiative recombination centers. Higgs et al.<sup>[7]</sup> indicate that no dislocation-related luminescence is observed from oxidation-induced stacking faults or epitaxial stacking faults grown under clean conditions; no metallic impurities were detected in the samples studied. This implies that the presence of

## 1. Introduction

Pushing the boundaries of silicon (Si) device miniaturization and functionality requires the understanding of defects, with a particular focus on their electrical and optical activity. Especially dislocations are crucial for engineering of advanced microelectronic devices and optimizing multicrystalline Si for the improvement of solar cell efficiency.<sup>[1]</sup> The study of the optical and electrical properties of dislocations is also important from the perspective of their potential use to develop a light source compatible with Si technology. The concept of such a light source based on dislocation networks has recently been demonstrated in refs. [2,3].


Dislocation-related recombination and luminescence in Si have been investigated for decades. The result was the observation of four dislocation-related emission peaks (D lines), currently

dislocations alone in Si does not necessarily result in luminescence. They also demonstrated<sup>[7]</sup> that intentional contamination of Si with these transition metals (Cu, Ni, Fe, Ag, and Au) leads to the emergence of dislocation luminescence features, including the D lines. The intensity of these features varies with the level of metal contamination, peaking at specific concentrations. This suggests that transition metals can modify the electronic states associated with dislocations, enhancing their ability to act as radiative recombination centers. Moreover, research by Kittler and Reiche<sup>[8]</sup> explains that “clean” dislocations, those that are not contaminated by impurities, show very small electrical activity when observed using electron beam-induced current techniques. This observation implies that the pure dislocation cores themselves, without any impurities or additional defects, do not significantly contribute to electrical activity.

The presence of the individual D lines and the ratio between their intensities were often dependent on how the dislocations were formed in the samples. Suezawa and Sumino<sup>[9]</sup> proposed that the reconstructed bonds along the dislocation core, rather than dangling bonds, are responsible for the observed photoluminescence (PL). Their studies indicate that reconstructed bonds, which result from the rearrangement of the Si lattice around dislocations, create the deep energy states responsible for the D lines emissions. According to the comprehensive work by Kittler and Reiche,<sup>[4]</sup> the D lines in the PL spectra are a result of the dislocation’s interaction with the crystal lattice and impurities. They suggest that these electronic states result from bond reconstruction in the dislocation’s core and reconstruction defects. The D lines are not only due to the presence of

D. Ryzhak, G. Kissinger, D. Spirito,<sup>[†]</sup> D. Kot  
IHP – Leibniz-Institut für innovative Mikroelektronik  
Im Technologiepark 25, 15236 Frankfurt (Oder), Germany  
E-mail: ryzhak@ihp-microelectronics.com

A. Ehlert, A. Sattler  
Siltronic AG  
Einsteinstraße 172, 81677 München, Germany

 The ORCID identification number(s) for the author(s) of this article can be found under <https://doi.org/10.1002/pssa.202400753>.

<sup>[†]</sup>Present address: BCMaterials, Basque Center for Materials, Applications and Nanostructures, UPV/EHU Science Park, 48940 Leioa, Spain

DOI: 10.1002/pssa.202400753

dislocations but also significantly influenced by the specific structure and the presence of point defects and impurities within the dislocation core.

On the other hand, the detailed analysis of the origin of D lines by Tajima<sup>[5]</sup> suggested that the 0.8 eV band comprises three components: two dislocation-related components ( $D_{a1}$  around 0.79 eV and  $D_{a2}$  around 0.94 eV) and an oxygen-precipitation-related component ( $D_b$  around 0.87 eV). These components reflect secondary defects or impurities trapped by the strain field around dislocations, the intrinsic nature of the dislocations themselves, and preferential oxygen precipitation on the dislocations, respectively. The D1 and D2 lines merge into a broadband termed  $D_{a1}$  with increasing temperature to about 150 K, and the  $D_b$  band becomes dominant at temperatures higher than 150 K. This behavior led to the assumption that the 0.8 eV band at room temperature originates predominantly from oxygen precipitates.

The D lines were widely investigated in the grain boundaries of multicrystalline Si as well as in the single-crystalline material.<sup>[10]</sup> Moreover, the dislocations were artificially formed during wafer bonding<sup>[11,12]</sup> and in spite of many investigations, the association of each D line to specific phenomena is still not well understood. The origin of the D1 and D2 lines was commonly attributed to secondary defects like metallic contaminations, oxygen precipitates, stress, or neighboring dislocations.<sup>[6]</sup> The origin of the D3 and D4 bands is instead closely associated with the intrinsic nature of dislocations within the crystal lattice.<sup>[13]</sup>

Our investigation delved into the characterization of Si dislocations across varying defect densities utilizing macro- and micro-PL techniques. In addition to this, we thoroughly examined the influence of nickel (Ni) contamination on dislocated Si wafers. Our comprehensive analysis extended to validating the consistency between PL results and etch pit observations, thereby establishing PL as a reliable technology for probing the effects of dislocations in Si wafers. This multifaceted approach provided deeper insights into the dislocation behavior and underscored the efficiency of PL as a tool for such investigations in semiconductor materials.

## 2. Experimental Section

In this study, dislocations were generated in one Si wafer during flash lamp annealing at temperatures close to the Si melting point for 20 ms. In order to generate a depth distribution of the dislocation density, the damage by wafer sawing was not removed prior to flash annealing. The Si wafer is boron-doped to a concentration of  $1.36 \times 10^{15} \text{ cm}^{-3}$ , achieving a resistivity of  $\approx 10 \text{ } \Omega\text{cm}$ .<sup>[14]</sup> The details of the sample annealing are described in ref. [15]. The Si wafer is characterized by a depth-dependent distribution of dislocations. **Figure 1** shows an optical microscopy cross-sectional view of the wafer after Secco etching for 3 min. In the cross section the top, center, and back parts of the sample, which were used for further PL analysis, are indicated. These sections exhibit different dislocation densities. The total height of the cross section is 900  $\mu\text{m}$ . The distribution of dislocations in terms of depth is clearly visible. The etch pits appear aligned along diagonal lines (Figure 1), which is attributed to the presence of slip lines. These slip lines are primarily along the  $\langle 110 \rangle$  directions, which are diagonally oriented relative

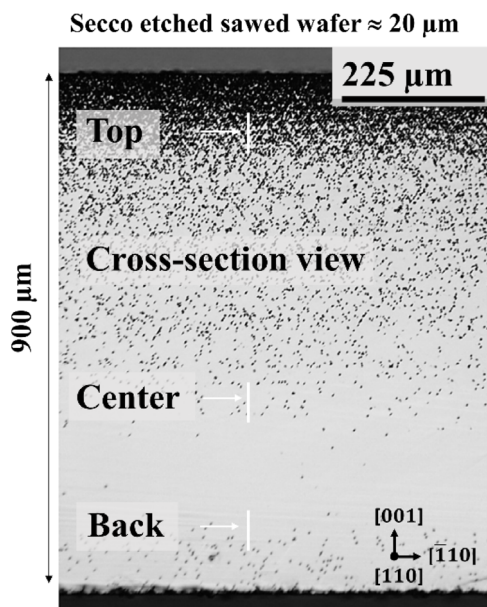


**Figure 1.** Cross-sectional view of a wafer after 3 min of Secco etching, showing the top, center, and back regions with a cross-sectional height of 900  $\mu\text{m}$ . Reprinted with permission.<sup>[15]</sup> Copyright 2015, The Electrochemical Society.

to the (001) plane. This alignment reflects the crystallographic slip systems in Si, where dislocations move along the  $\{111\}$  slip planes and the  $\langle 110 \rangle$  directions.

To assess the impact of dislocation densities on D lines, we performed various measurements. For macro- and micro-PL measurements, the samples were analyzed in top view. Therefore, the samples were polished to various depths and etched with a mixture of hydrofluoric and nitric acid to remove saw and polishing damages. The samples obtained in this way were characterized by different dislocation densities. Another sample was cleaved and the measurements were carried out on the cross-sectional top for micro-PL. In all cases, the dislocation density was determined after Secco etching for 3 min. The samples and their corresponding densities/orientation are included in **Table 1**. It is reasonable to assume that the sawing step introduced contamination. We performed time-of-flight secondary ion mass spectrometry (ToF-SIMS) before sawing and etching of the wafer to monitor contamination level, using an IONTOF system, and no contamination was detected, as it was below the measurements detection limit of about  $2 \times 10^{10} \text{ cm}^{-2}$ . In order to monitor Ni concentration in Ni-contaminated samples (Table 1), ToF-SIMS was also used. PL measurements were performed with a HORIBA iHR 320 spectrometer equipped with a Synapse/Symphony InGaAs II detector, with excitation at 532 nm wavelength. A micro-PL setup with a 50x objective with  $\approx 1 \mu\text{m}$  spot and 11.3 mW power ( $2 \times 10^6 \text{ W cm}^{-2}$ ) was used, as well as a closed-cycle compression cryostat macro-PL setup with  $\approx 1 \text{ mm}$  spot size with 0.18 W power ( $32 \text{ W cm}^{-2}$ ). To establish the temperature dependence, for micro-PL measurements we used a liquid flow cryostat from Advanced Research Systems model LT-3-110, which had cooldown temperatures reaching  $\approx 4.2 \text{ K}$  when using liquid helium and 77 K for nitrogen.

**Table 1.** Description of samples with corresponding dislocation density  $N_{\text{Dis}}$ .

Sample $N_{\text{Dis}}$ [ $\text{cm}^{-2}$ ]	Orientation	Description
$5.4 \times 10^6$	Top view (at 106 $\mu\text{m}$ depth of Figure 1)	Etched
$3.6 \times 10^5$	Top view (at 290 $\mu\text{m}$ depth of Figure 1)	Etched
$2.4 \times 10^5$	Top view (at 450 $\mu\text{m}$ depth of Figure 1)	Etched
$1.4 \times 10^7$	Cross section	–
$2 \times 10^7$	Top view	No contamination
$2 \times 10^7$	Top view	Contaminated ( $\text{Ni } 5 \times 10^{12} \text{ cm}^{-2}$ )
$2 \times 10^7$	Top view	Contaminated ( $\text{Ni } 5 \times 10^{12} \text{ cm}^{-2}$ ) + annealed

Macro-PL measurements were conducted using a Janis closed cycle refrigerator system, with a base temperature  $\approx 10$  K. These systems enable a wide variety of optical experiments to be performed between  $\approx 8$  and 325 K.

### 3. Results and Discussion

Using the macro-PL setup, the sample with the highest dislocation density (106  $\mu\text{m}$  depth) was studied at different temperature (Figure 2). At 13 K, clear and sharp D lines were observed, alongside of band-to-band (BB) and BB phonon replica (BBPR)

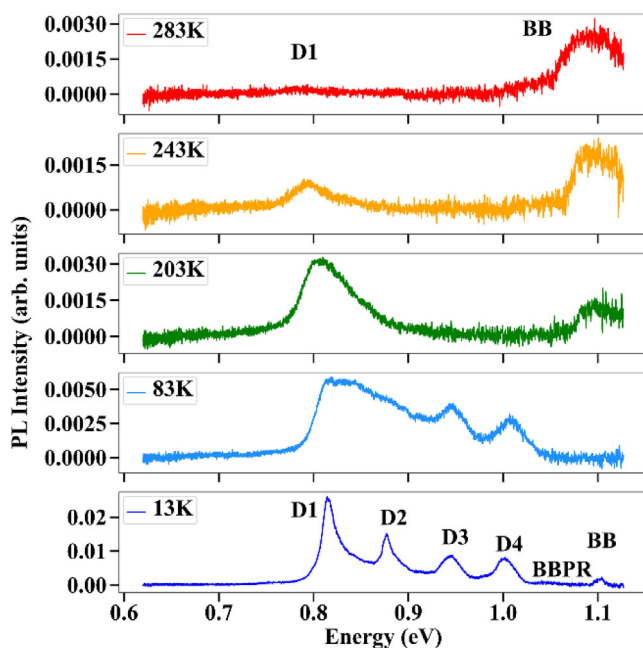


**Figure 2.** Macro-PL temperature dependence spectra of Si dislocation density  $N_{\text{Dis}} = 5.4 \times 10^6 \text{ cm}^{-2}$ .

(Figure 2). As the temperature rises, these peaks broaden and diminish, and eventually merge ( $\approx 200$  K) into a broadband emission at 0.8 eV due to increased interaction with phonons, which provide additional pathways for nonradiative recombination. The high-temperature PL spectra tend to be dominated by BB transitions at  $\approx 1.1$  eV, which are less sensitive to dislocations and defects. Around room temperature (283 K), the PL intensity is generally weak, and the dislocation-related peaks have merged into the background, making BB transitions more dominant. We thus focus on low-temperature measurements to investigate the D lines.

The images in Figure 3 show optical microscopy pictures of Si wafer surfaces with varying density of dislocations, along with their corresponding macro-PL spectra at 13 K. Figure 3a displays a Si wafer surface with the highest dislocation density (106  $\mu\text{m}$  depth), as evidenced by the dark features (etch pits). The dislocation density decreases in Figure 3b,c, with densities of  $N_{\text{Dis}} = 3.6 \times 10^5$  and  $N_{\text{Dis}} = 2.4 \times 10^5 \text{ cm}^{-2}$  (290 and 450  $\mu\text{m}$  depth), respectively, showing a visible reduction in the number of etch pits. In the corresponding PL spectra (Figure 3d–f), the presence of BB, BBPR, and sub-bandgap emission was detected. The latter ones were identified as the previously mentioned D1, D2, D3, and D4 lines.<sup>[4]</sup> All peak positions, despite different defect density, remain nearly constant. Figure 3d, corresponding to the highest dislocation density (the same as in the bottom panel of Figure 2), shows the highest D line intensity and the lowest BB and BBPR intensities. The high density of dislocations provides numerous localized states within the bandgap that act as efficient traps for charge carriers.<sup>[16]</sup> Consequently, the charge carriers recombine at these localized dislocation states, leading to intense D line emissions and suppressed BB and BBPR emissions due to the lack of free carriers available for these transitions. With lower dislocation density (Figure 3e,f), the D line intensity decreases and the BB and BBPR emissions are more pronounced. Additionally, a shoulder near the BB peak (Figure 3e,f) indicates recombination at 1.078 eV assigned to boron dopants, likely corresponding to a free-to-bound recombination, where a free electron from the conduction band recombines with a hole bound to a boron dopant.<sup>[17,18]</sup>

The D lines were analyzed by Gaussian fitting and performing background subtraction. Variations in PL intensity (defined as the peak height), depicted in Figure 4, highlight the differences in the PL band responses. In Figure 4, we present PL intensities of D1, D2, D3, and D4 bands as ratios to the total intensity sum of all bands to compare the relative contribution of each band. It can be observed that the decrease in band normalized intensity is varying across different bands. Normalized PL intensities of D1 and D2 decrease with decreasing the dislocation density (Figure 4), demonstrating a different trend compared to D3 and D4, which increase. The observation of the different normalized PL intensities behavior in Figure 4 showed that D1 and D2 have a different origin than D3 and D4. D1 and D2 could be related to secondary defects, potentially due to stress or nearby dislocations, while D3 and D4 represent their intrinsic properties of the dislocation.<sup>[19]</sup>

We also measured micro-PL at 4.5 K (Figure 5) for the samples with  $N_{\text{Dis}} = 5.4 \times 10^6$  and  $N_{\text{Dis}} = 3.6 \times 10^5 \text{ cm}^{-2}$ . The PL relative intensity for D1, D2, and D3 lines is lower in the micro-PL (Figure 5) compared to the macro-PL (Figure 3d,e). However,



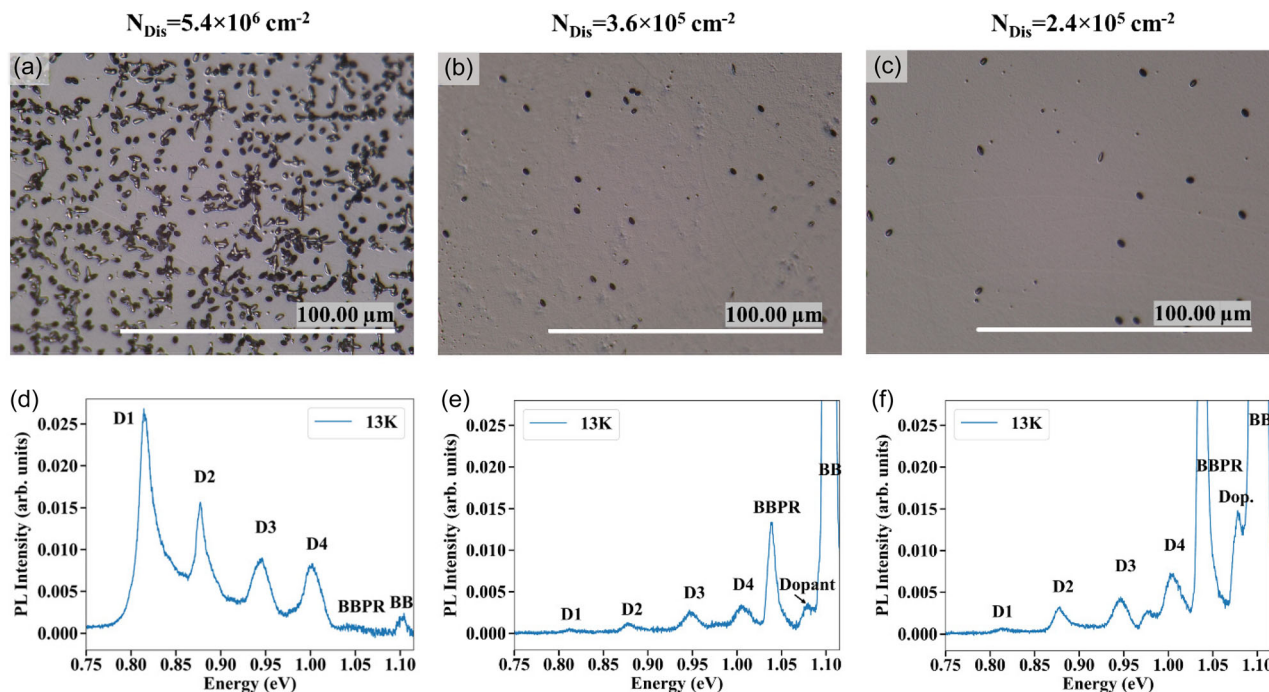


**Figure 3.** a–c) Optical microscopy pictures and d–f) macro-PL spectra at 13 K of various densities of dislocation  $N_{Dis} = 5.4 \times 10^6 \text{ cm}^{-2}$  (a,d),  $N_{Dis} = 3.6 \times 10^5 \text{ cm}^{-2}$  (b,e), and  $N_{Dis} = 2.4 \times 10^5 \text{ cm}^{-2}$  (c,f).

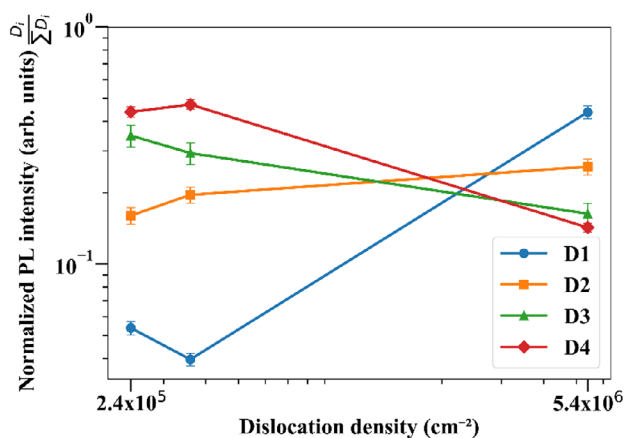


**Figure 4.** PL intensity of D lines versus dislocation density, reported as normalized to their sum.

the D4 line exhibits higher intensity in the micro-PL and merges with BBPR at high dislocation densities. This behavior can be attributed to the spatial resolution differences between micro- and macro-PL measurements, as well as difference in power density between the two setups. Micro-PL has higher spatial resolution and can detect localized regions with higher dislocation densities, leading to a stronger signal from defects like D4. At higher dislocation densities, the D4 line merges with a small shoulder near 1.04 eV. This shoulder, referred to as BBPR, becomes more prominent at lower dislocation densities. Higher dislocation densities tend to minimize the BBPR shoulder due to increased nonradiative recombination, while lower

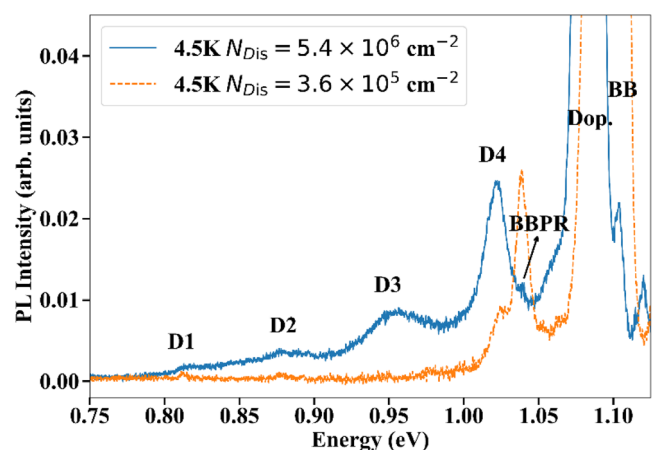


**Figure 5.** Micro-PL spectra at 4.5 K for  $N_{Dis} = 5.4 \times 10^6 \text{ cm}^{-2}$  and  $N_{Dis} = 3.6 \times 10^5 \text{ cm}^{-2}$  dislocation densities.

densities allow for clearer observation of both defect-related lines and BB recombination. Also, it should be noted that the D1 and D2 lines, indicative of secondary defects, are prominently observed in macro-PL (Figure 3d), reflecting a widespread dislocation distribution, but become almost imperceptible under micro-PL's finer focus (Figure 5), suggesting that these defects are relatively small and nonlocalized within the Si lattice, in contrast with those associated to D4 and D3 lines.

To investigate any variations across the sample, we mapped the PL intensities across the  $N_{Dis} = 5.4 \times 10^6 \text{ cm}^{-2}$  sample (106  $\mu\text{m}$  depth). A line scan, indicated by the red line on Figure 6a, was performed across a region with separated

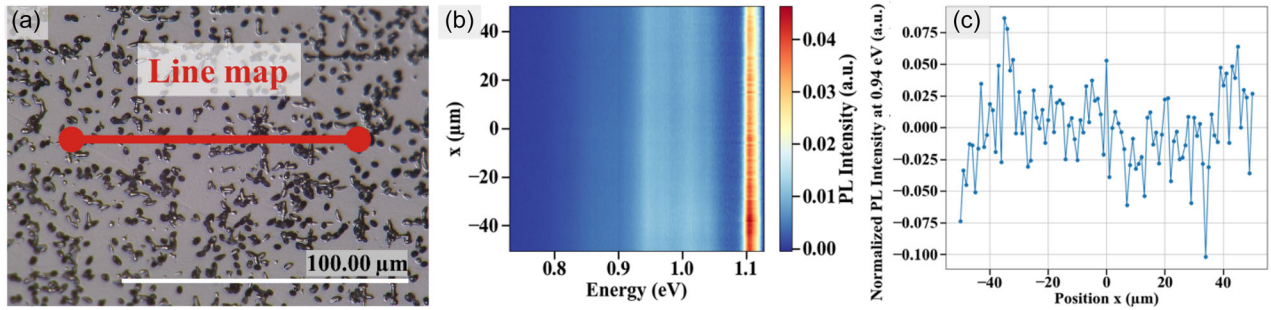


**Figure 6.** Micro-PL mapping for the sample with  $N_{\text{Dis}} = 5.4 \times 10^6 \text{ cm}^{-2}$ . a) Optical microscopy picture (the red line marks the scan region), b) color map of the PL intensity at 80 K as a function of location and energy, and c) normalized PL intensity at 0.94 eV (D3 line at 80 K) as a function of position.

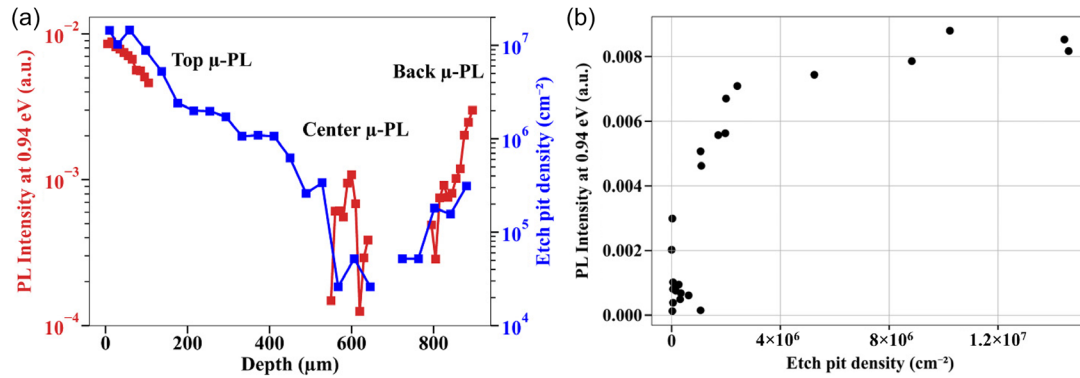


**Figure 7.** a) Comparison of the etch pit density and micro-PL at 80 K intensity of D3 line as a function of the depth. b) Depth dependence of the etch pit density and micro-PL intensity of D3 at 80 K.

dislocations pits as visible in the optical microscopy image. The resulting map shown in Figure 6b, with the left vertical axis corresponding to the horizontal scan line in Figure 6a, presents the PL intensity as a function of position and energy. The observation of a uniform PL response along the scanned line suggests that the luminescence is not dependent on the surface defect variations. Instead, it indicates that the laser penetration, which has a depth of  $\approx 1 \mu\text{m}$ , leads to excitation of the secondary defects below the surface, resulting in nearly uniform D line intensities (Figure 6c). The intensities shown in Figure 6c were normalized by dividing each value by the highest intensity value. The observed noise (negative values) in the data is primarily attributed to a shift in focus that occurred during the measurement process.

We also performed a comparison of micro-PL results and etch pit density against the depth with  $N_{\text{Dis}}$  up to  $1.4 \times 10^7 \text{ cm}^{-2}$ . Figure 7a reports the micro-PL results of absolute intensity of the D3 line (left y-axis) and the etch pit density (right axis), which is proportional to the dislocation density. The micro-PL intensity and the etch pit density data follow a similar trend for the top part of the sample (depth 0–900  $\mu\text{m}$ ), decreasing sharply with depth, vary in the central part (with an increase followed by a decrease), and increase in the bottom part.

This suggests that the defects responsible for the D3 line are associated with dislocations within the sample. The correlation plot between PL intensity and etch pit density (Figure 7b) shows that above  $N_{\text{Dis}} = 5 \times 10^6 \text{ cm}^{-2}$  the PL intensity saturates. The

nonlinear behavior of the PL intensity versus etch pit density could be due to the presence of other defects, and to the quality of the crystal lattice around the dislocations, that reduce the radiative recombination efficiency, or to an increased absorption of the excitation laser.

As discussed in the introduction, metal contamination has been associated with the D lines. Figure 8 shows macro-PL

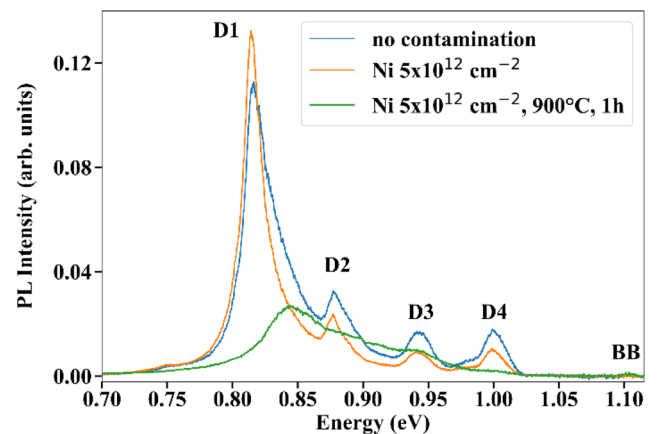


**Figure 8.** Macro-PL spectra at 13 K of samples ( $N_{\text{Dis}} > 2 \times 10^7 \text{ cm}^{-2}$ ) with and without Ni contamination ( $5 \times 10^{12} \text{ cm}^{-2}$ ), and with Ni annealed for 1 h.

spectra at a low temperature of 13 K for Si samples with a high dislocation density (greater than  $2 \times 10^7 \text{ cm}^{-2}$ ), without and with Ni contamination ( $5 \times 10^{12} \text{ cm}^{-2}$  as a surface density) and for the contaminated sample after being annealed for 1 h at 900 °C. The spectra without and with Ni contamination show the presence of D1, D2, D3, D4, and BB lines. However, in the annealed samples, the D lines are no longer recognizable, and a broadband appears, which could be attributed to defects. The observed changes in the PL spectra align with the findings of Higgs et al.<sup>[7]</sup> suggesting that Ni contamination affects the electronic states associated with dislocations. The intensity reduction and the shift in the postannealing spectra could indicate mechanisms such as oxygen and nickel silicide precipitation.

## 4. Conclusions

Using PL techniques, our results confirm the identification of defects associated with D lines, demonstrating that PL is effective in distinguishing dislocation density. Our study demonstrates that micro-PL effectively highlights localized defect behaviors such as the pronounced D4 line, which represent the intrinsic properties of the dislocation. In contrast, macro-PL indicates the widespread distribution of secondary defects, likely due to stress or nearby dislocations, illustrating the complementary roles of macro- and micro-PL in characterizing material defects.

We also showed that PL techniques enable the monitoring of changes along the depth of samples, establishing a relationship with etch pit density. Knowing how the dislocations vary throughout the material by using PL methods can lead to strategies to reduce their effects, such as specific annealing processes or choosing an appropriate stacking sequence of layers for device fabrication.

## Acknowledgements

The authors would like to thank Joel Rauscher, engineer, for his technical support.

## Conflict of Interest

The authors declare no conflict of interest.

## Author Contributions

**Diana Ryzhak:** conceptualization (lead); data curation (lead); formal analysis (lead); investigation (lead); visualization (lead); writing—original draft (lead). **Gudrun Kissinger:** validation (supporting); writing—review and editing (supporting). **Andreas Ehlert:** validation (supporting); writing—review and editing (supporting). **Andreas Sattler:** validation (supporting); writing—review and editing (supporting). **Davide Spirito:** supervision (supporting); validation (supporting); writing—

review and editing (supporting). **Dawid Kot:** conceptualization (supporting); funding acquisition (lead); resources (supporting); supervision (lead); validation (lead); writing—review and editing (lead).

## Data Availability Statement

Research data are not shared.

## Keywords

D lines, defect characterization, dislocations, micro-photoluminescence, Si

Received: September 20, 2024

Revised: November 29, 2024

Published online: December 22, 2024

- [1] H. J. Möller, C. Funke, D. Kreßner-Kiel, S. Würzner, *Energy Procedia* **2011**, 3, 2.
- [2] M. Kittler, M. Reiche, W. Seifert, X. Yu, T. Arguirov, O. Vyvenko, T. Mchedlidze, T. Wilhelm, *ECS Trans.* **2006**, 3, 429.
- [3] T. Arguirov, M. Kittler, W. Seifert, X. Yu, M. Reiche, *Mater. Sci. Eng., B* **2006**, 134, 109.
- [4] M. Kittler, M. Reiche, in *Crystalline Silicon - Properties and Uses* (Ed: S. Basu), InTech, Rijeka, Croatia **2011**, <https://doi.org/10.5772/22902>.
- [5] M. Tajima, *IEEE J. Photovoltaics* **2014**, 4, 1452.
- [6] H. Sugimoto, M. Inoue, M. Tajima, A. Ogura, Y. Ohshita, *Jpn. J. Appl. Phys.* **2006**, 45, L641.
- [7] V. Higgs, E. C. Lightowers, C. E. Norman, P. Kightley, *Mater. Sci. Forum* **1992**, 83–87, 1309.
- [8] M. Kittler, M. Reiche, *Adv. Eng. Mater.* **2009**, 11, 249.
- [9] M. Suezawa, K. Sumino, *J. Phys. Colloq.* **1983**, 44, C4-133.
- [10] M. Trempa, G. Müller, J. Friedrich, C. Reimann, in *Handbook of Photovoltaic Silicon* (Ed: D. Yang), Springer, Berlin, Heidelberg **2018**, pp. 1–48, [https://doi.org/10.1007/978-3-662-52735-1\\_25-1](https://doi.org/10.1007/978-3-662-52735-1_25-1).
- [11] M. Reiche, *Mater. Sci. Forum* **2008**, 590, 57.
- [12] S. Bao, Y. Wang, K. Lina, L. Zhang, B. Wang, W. A. Sasangka, K. E. K. Lee, S. J. Chua, J. Michel, E. Fitzgerald, C. S. Tan, K. H. Lee, *J. Semicond.* **2021**, 42, 023106.
- [13] H. T. Nguyen, F. E. Rougieux, F. Wang, H. Tan, D. Macdonald, *IEEE J. Photovoltaics* **2015**, 5, 799.
- [14] G. Kissinger, D. Kot, M. Lisker, A. Sattler, *ECS J. Solid State Sci. Technol.* **2019**, 8, N79.
- [15] G. Kissinger, D. Kot, M. A. Schubert, A. Sattler, *ECS J. Solid State Sci. Technol.* **2015**, 4, P195.
- [16] V. V. Kveder, Y. A. Osipyan, W. Schröter, G. Zoth, *Phys. Status Solidi A* **1982**, 72, 701.
- [17] A. Liu, H. T. Nguyen, D. Macdonald, *Phys. Status Solidi A* **2016**, 213, 3029.
- [18] P. J. Dean, J. R. Haynes, W. F. Flood, *Phys. Rev.* **1967**, 161, 711.
- [19] H. T. Nguyen, F. E. Rougieux, F. Wang, D. Macdonald, *Energy Procedia* **2015**, 77, 619.